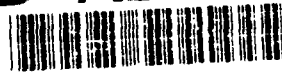


AD-A237 261



OFFICE OF NAVAL RESEARCH

R&T Code 413a001

Technical Report No. 2

Photochemistry of Dimethyl Cadmiun
on Quartz and Silicon Surfaces

by

S.-P. Lee and M. C. Lin

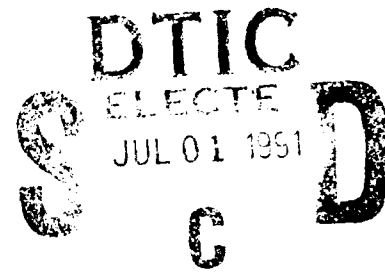
Prepared for Publication

in

Appl. Phys. (B),

Reproduction in whole or in part is permitted for any purpose of the
United States Government

This document has been approved for public release and sale;
its distribution is unlimited.



91 6 24 07 2

91-03246



Photochemistry of Dimethyl Cadmiun
on Quartz and Silicon Surfaces

S.-P. Lee and M. C. Lin
Department of Chemistry
Emory University
Atlanta, GA 30322

REPORT DOCUMENTATION PAGE

1a. REPORT SECURITY CLASSIFICATION Unclassified		1b. RESTRICTIVE MARKINGS N/A	
2a. SECURITY CLASSIFICATION AUTHORITY N/A		3. DISTRIBUTION/AVAILABILITY OF REPORT Approved for public release; distribution unlimited.	
2b. DECLASSIFICATION/DOWNGRADING SCHEDULE N/A		5. MONITORING ORGANIZATION REPORT NUMBER(S) N00014-89-J-1235	
4. PERFORMING ORGANIZATION REPORT NUMBER(S)		7a. NAME OF MONITORING ORGANIZATION Office of Naval Research (Code 413)	
6a. NAME OF PERFORMING ORGANIZATION Emory University	6b. OFFICE SYMBOL (If applicable)	7b. ADDRESS (City, State and ZIP Code) Chemistry Program 800 N. Quincy Street Arlington, Virginia 22217	
6c. ADDRESS (City, State and ZIP Code) Department of Chemistry 1515 Pierce Drive Atlanta, GA 30322	8a. NAME OF FUNDING/SPONSORING ORGANIZATION Office of Naval Research	8b. OFFICE SYMBOL (If applicable)	9. PROCUREMENT INSTRUMENT IDENTIFICATION NUMBER
8c. ADDRESS (City, State and ZIP Code) Chemistry Program 800 N. Quincy Street, Arlington VA 22217	10. SOURCE OF FUNDING NOS.		
11. TITLE (Include Security Classification) Photochemistry of Dimethyl Cadmium on Quartz and Si(111) Surfaces	PROGRAM ELEMENT NO.	PROJECT NO.	TASK NO. WORK UNIT NO.
12. PERSONAL AUTHOR(S) S.P. Lee and M. C. Lin			
13a. TYPE OF REPORT Interim Technical	13b. TIME COVERED FROM 6/1/90 to 5/31/91	14. DATE OF REPORT (Yr. Mo., Day) February 26, 1991	15. PAGE COUNT 53
16. SUPPLEMENTARY NOTATION Prepared for publication in Appl. Phys. B. (Photophysics and Laser Chemistry)			
17. COSATI CODES		18. SUBJECT TERMS (Continue on reverse if necessary and identify by block number)	
FIELD	GROUP	SUB. GR.	
		Photochemistry of (CH ₃) ₂ Cd, LCVD on Quartz and Si(111) substrates, Mechanism of (CH ₃) ₂ Cd photofragmentation	
19. ABSTRACT (Continue on reverse if necessary and identify by block number)			
<p>The photochemistry of adsorbed dimethyl cadmium at submonolayer levels on a fused quartz and a Si(111) single crystal surface has been investigated at 193 and 248 nm using a rare-gas fluoride excimer laser. The desorbed gaseous products, which include CH₂, CH₃, CH₄, C₂H₄, C₂H₅, C₂H₆, Cd, CH₃Cd and (CH₃)₂Cd, have been detected by time-of-flight mass spectrometry by means of either electron impact or resonance-enhanced multiphoton ionization. The translational energies of these desorption products could be characterized in terms of Maxwell-Boltzmann temperatures, TMB's, which depend strongly on sample dosage (surface coverage), laser fluence, photon energy and the nature of the substrates employed. The TMB's of the C₁- and C₂- hydrocarbon species were found to be much lower than those of Cd, CH₃Cd and (CH₃)₂Cd, suggesting that the electronic excitation/relaxation mechanism may be involved in the desorption of these metal/metal-containing species. A similar mechanism is not available for the desorption of the hydrocarbon products. A realistic mechanism is proposed for the UV-photochemistry of adsorbed (CH₃)₂Cd.</p>			
20. DISTRIBUTION/AVAILABILITY OF ABSTRACT UNCLASSIFIED/UNLIMITED <input checked="" type="checkbox"/> SAME AS RPT. <input type="checkbox"/> DTIC USERS <input type="checkbox"/>		21. ABSTRACT SECURITY CLASSIFICATION Unclassified	
22a. NAME OF RESPONSIBLE INDIVIDUAL Dr. David L. Nelson		22b. TELEPHONE NUMBER (Include Area Code) (202) 696-4410	22c. OFFICE SYMBOL

Abstract

The photochemistry of adsorbed dimethyl cadmium at submonolayer levels on a fused quartz and a Si(111) single crystal surface has been investigated at 193 and 248 nm using a rare-gas fluoride excimer laser. The desorbed gaseous products, which include CH_2 , CH_3 , CH_4 , C_2H_4 , C_2H_5 , C_2H_6 , Cd , CH_3Cd and $(\text{CH}_3)_2\text{Cd}$, have been detected by time-of-flight mass spectrometry by means of either electron impact or resonance-enhanced multiphoton ionization. The translational energies of these desorption products could be characterized in terms of Maxwell-Boltzmann temperatures, T_{MB} 's, which depend strongly on sample dosage (surface coverage), laser fluence, photon energy and the nature of the substrates employed. The T_{MB} 's of the C_1 - and C_2 - hydrocarbon species were found to be much lower than those of Cd , CH_3Cd and $(\text{CH}_3)_2\text{Cd}$, suggesting that the electronic excitation/relaxation mechanism may be involved in the desorption of these metal/metal-containing species. A similar mechanism is not available for the desorption of the hydrocarbon products. A realistic mechanism is proposed for the UV-photochemistry of adsorbed $(\text{CH}_3)_2\text{Cd}$.

PACS: 82.50, 82.65NZ



Accession For	
AT	GRAND <input checked="" type="checkbox"/>
BTIC Tab	<input type="checkbox"/>
Unrecorded	<input type="checkbox"/>
Justification	
By	
Distribution/	
Availability Codes	
Dist	Avail and/or Special
A-1	

INTRODUCTION

Dimethyl cadmium (DMCd) is an important organometallic source molecule for the deposition of cadmium sulfide, telluride and other compound II/VI semiconductors by LCVD (laser chemical vapor deposition) or OMCVD (organometallic CVD) [1-3]. The photochemistry of DMCd in the gas phase has also been a subject of considerable current interest.

Spectroscopic studies of the excited states of DMCd in the UV[4-7] and VUV [6,7] regions of the spectrum have been made recently by many groups. The absorption in the UV region begins near 270 nm, appearing as a broad, featureless band which increases sharply below 230 nm with regular structures [4-7]. The broad, continuous absorption in the lower energy regime has been attributed to excitation to the first excited, triplet state (which is bent) according to Amirav et al. [5], instead of a singlet-singlet transition, as was proposed by Chen and Osgood [4]. The stronger absorption peaking near 215 nm is now commonly accepted as due to the $\tilde{X}^1\Sigma_g^+ - \tilde{B}^1\pi_u$ transition [4,5].

The photodissociation of DMCd in the \tilde{B} state has been shown to produce CH_3 and CH_3Cd ($\tilde{A}^2\Sigma$), which fluoresces in the 440-445 nm region [5,6,8]. The CH_3 radical was measured to carry an average translational energy of 24 kJ/mole when DMCd was photolyzed at 193 nm [8]. Interestingly, a similar study made at 248 nm resulted in no detectable fragmentation, although the absorption cross section at this wavelength is half as strong as that at 193 nm [4-7] and the photon energy is more than sufficient to break both C-Cd bonds.

Our present interest lies in the elucidation of the mechanism of the photodissociation of DMCd adsorbed on solid surfaces in relation to the LCVD of Cd. The first attempt to deposit Cd films on solid surfaces was made by Deutsch, Ehrlich, and Osgood [2,9], who used a cw UV-laser at 257 nm to

irradiate the surface directly in a static cell containing 1-10 torr of DMCd. Under their conditions, the excitation of DMCd in both gaseous and adsorbed phases can promote photochemical decomposition reactions. Accordingly, the photochemistry is far more complex than the laser-induced dissociation of adsorbed DMCd in vacuum, in which secondary reactions of desorbed, gas-phase species with the surface and the complications by other physicochemical processes, including surface heating by cw radiation, can be avoided. As a first step toward the understanding of the complex deposition process for practical applications, we have carried out a study of the photodissociation of adsorbed DMCd in vacuum under sub-monolayer conditions, using a time-of-flight mass spectrometric (TOF-MS) method. Both the conventional electron impact ionization (EI) and the resonance-enhanced multiphoton ionization (REMPI) techniques were employed for molecular as well as transient (atomic and radical) species detection. We have examined the differences in surface photochemistry induced by different photon energies, laser powers, DMCd coverages, as well as the nature of the substrates employed.

1. Experimental

The experimental setup is essentially the same as the one employed before [10-12]. The laser photolysis/time-of-flight measurement system consists of two chambers separated by a 3-mm skimmer. The surface photolysis chamber was pumped by a 1000 l/s Diffstak (Edwards) diffusion pump, which was separated from the chamber with a gatevalve. The analysis chamber, which housed an Extrel C-50 quadrupole mass spectrometer (QMS), was evacuated with a 1000 l/s Leybold turbomolecular pump. After a proper

bakeout, the background pressures were typically 1×10^{-8} and 5×10^{-9} torr in the photolysis and mass spectrometer chambers, respectively.

The solid sample [25-mm diameter fused quartz or Si(111)] was mounted in the photolysis chamber using a brass ring welded onto a copper block, which was directly attached to a liquid-N₂ reservoir. The copper block could also be heated up to 400 K before each photolytic experiment to remove any possible volatile impurities from the solid surface. The substrate was typically aligned normal to the skimmer-QMS analysis axis and interacted with the photolysis laser beam at a 10° glazing angle. The distance between the substrate and the center of the ionization region of the QMS was measured to be 13 cm.

The photolysis laser (Lambda Physik EMG-102 MSC) was operated at either 193 nm (ArF) or 248 nm (KrF). The energy of the laser could be varied from several mJ/pulse to 30 mJ/pulse, with a typical photolysis energy of about 20 mJ/pulse covering a rectangular area of about 1 cm² across the center of the surface.

The dimethyl cadmium sample (10% DMCd in He) was dozed onto the cold substrate (whose temperature could be varied from 140 - 400 K) through a stainless steel capillary tube held 2 cm away from the surface at a 45° angle. The flow rate of the gas mixture was controlled by a needle valve in conjunction with a mass flow meter (MKS type 258 B). During an experimental run, the pressure in the source chamber was typically maintained at $< 10^{-6}$ torr and the repetition rate of the photolysis laser kept at 3 Hz which allowed us to have < 0.1 L (Langmuir = 10^{-6} torr.sec) dosage between laser shots.

The detection of the desorbed photolysis products by QMS could be achieved by either electron impact ionization or REMPI (resonantly enhanced multiphoton ionization). For REMPI/TOF detection, an excimer laser pumped dye laser (Lambda Physik EMG 201MSC and FL3002) was guided with two 90°

prisms and focused at the center of the ionization region through a 15-cm focal-length lens. Typical outputs of the dye laser were 3 mJ/pulse for CH₃ and 8 mJ/pulse for Cd detection using p-terphenyl dye.

Ions were collected and amplified through a channeltron ion multiplier. The outputs from the channeltron were further amplified using a fast response pulse-amplifier (Thorn EMI Type C632) and monitored using either a 100 MHz digital storage oscilloscope (Nicolet Model 450 Waveform Acquisition System) for EI/TOF detection or a gated integrator and boxcar signal averaging system (Stanford Research Model 250 and 245) controlled by computer (IBMPC-AT) for REMPI/TOF detection and REMPI spectrum acquisition. A multichannel digital delay/pulse generator (Stanford Research Model DG535) was used to synchronize the photolysis excimer laser, the dye laser, and the data acquisition system (boxcar etc.). The delayed trigger-pulse to the dye laser could be varied to scan TOF profiles for REMPI/TOF or fixed at TOF peaks for REMPI spectral acquisition. The natural abundances of Cd isotopes are 12.25% of Cd¹¹⁰, 24.17% of Cd¹¹², and 28.73% of Cd¹¹⁴. In our experiment, we were able to observe those ratios but our results and discussion were based only on the most abundant isotope (Cd¹¹⁴).

Both CH₃ and Cd can be readily detected by REMPI in the 330 - 340 nm range of the spectrum. The CH₃ radical was ionized by (2+1) REMPI at 333.4 nm via the resonance state $3p^2A_2''$ [13]. For spectral scans of the desorbed CH₃ fragment, the probing dye laser was delayed variably between 160 and 225 μ sec after photodissociation. The boxcar gate was set at 28 μ sec after the dye laser pulse.

Cd could also be detected by (2+1) REMPI via $5d\ ^1D_2$ at 337.7 nm, $5d\ ^3D_J$ ($J = 0, 1, 2$) at 336.0 - 336.2 nm as well as $6p\ ^1P_1$ at 333.8 nm [14]. For its spectral

scans, the dye laser was delayed by about 360 μ sec after photolysis pulse, with a boxcar gate opened at 74 μ sec following the dye laser pulse.

2. Results

The overall pictures of photodesorption/photofragmentation of DMCd adsorbed on SiO₂ and Si(111) substrates, photolyzed at both 193 and 248 nm, are shown in Figs. 1 and 2 in terms of the TOF-profiles of various species. Signals obtained with the Si(111) surface were noted to be much stronger due perhaps to a stronger DMCd adsorption and a stronger absorption of the UV radiation as well. Dots shown in Fig. 1 represent the experimental data and the fitted Maxwell-Boltzmann distributions were superimposed as solid lines. All of these profiles have been corrected for the transit time through the quadrupole mass spectrometer and they represent the time-of-arrival of those species at the electron-impact ionizer, accordingly, if any of them derived from the cracking of heavier molecules by electron bombardment, their TOF profiles should resemble those of their parent profiles.

It is easy to see from these profiles that almost all of the observed species carry slightly different translational energies, suggesting that a lot of photofragmentation processes occur at the surface. The fitted Maxwell-Boltzmann translational temperatures (T_{MB}) of various species from the photolysis on the quartz substrate are summarized in Tables 1 and 2. The TOF-profiles of various ions shown Fig. 2 obtained with the Si(111) surface are mostly non-Maxwellian. They cannot be characterized with a single T_{MB} .

The extent of photofragmentation depends strongly on the energies of laser photon as shown in Figs. 3 and 4, in which the total ion count of each fragment normalized with respect to the parent count is compared for both SiO₂

and Si substrates photolyzed at 193 and 248 nm. The results clearly illustrate the significant effect of photon energy and, to a less significant extent, the nature of substrates on the photofragmentation of DMCd. The effect of photon energy may be attributed to the difference in both absorptivity and fragmentation pathways. At 193 nm, it is possible to excite both the first and the second excited state of DMCd, while at 248 nm only the first excited state can be reached. Both excited states are repulsive, giving rise to dissociation products with slightly different internal energy distributions as will be discussed later.

The informations on how the adsorbed species react under different conditions, such as surface coverage, excitation energy and fluence, etc. should be helpful for the characterization of photodissociation processes at the surface. In the following sections, the effects of these varying conditions on fragmentation and desorption dynamics will be discussed.

2.1. Photodesorption of DMCd

2.1.1. Coverage dependence

The dependence of the photodesorption of DMCd on its coverage over the quartz and silicon surfaces has been examined by changing the pulsing rate of the laser radiation. The repetition rate was varied from 0.1 to 20 Hz at a constant pressure (lower than 10^{-6} torr of the DMCd mixture) with a steady flow rate of 0.2 mcc/sec, so that the exposure is given in units of Langmuir. Both quartz and Si(111) substrates were examined under similar conditions. Unless specified otherwise, all experiments were carried out with the exposure of 0.030 L for the quartz substrate and 0.024 L for the Si(111) substrate.

The representative TOF profiles of DMCd from the quartz surface at different exposures are compared in Fig. 5, showing typical changes of most probable energies in time and total desorption counts. Again, the dots are experimental data point and the superimposed solid lines were the fitted Maxwell-Boltzmann distributions. Both the translational temperature and total desorption yields were found to increase quite linearly with increasing exposures up to 0.1 L, above which deviation from the linearity occurs. These coverage-dependence results are summarized in Figs. 6A and 6B for quartz and Si(111) substrates, respectively. Although the quartz and silicon surface results are similar, both T_{MB} and the photon yield from the Si(111) surface are much higher. However, the initial rate of increase in T_{MB} with exposure on the Si surface appeared to be somewhat slower than that of the quartz surface.

2.1.2. Dependence on laser wavelength and fluence

The dependence of the DMCd desorption yield on photon energy and laser fluence is shown in Figs. 7 and 8 for the quartz substrate. These experiments were carried out with the available intensity ranges of the 193 and 248 nm radiations. At the same fluence, the photon yield with the 248 nm radiation was substantially smaller than that with 193 nm, presumably because of the lower absorptivity of DMCd at the former wavelength as discussed earlier. Because of that reason, the experiment was carried out at higher fluences with the 248 nm radiation.

The results obtained with both wavelengths presented in Figs. 7 and 8 show changes in total desorption counts and translational energy distributions with the laser fluence. Both quantities increase rapidly with fluence and reach plateau values at fluences higher than 17 mJ/cm².pulse at 193 nm and 25

mJ/cm².pulse at 248 nm. Similar results were found for other desorbed fragments as presented in Tables 1 and 2.

Figures 9A and 9B summarize measured ion counts for various fragments as functions of laser fluence for both SiO₂ and Si surfaces irradiated at 193 and 248 nm.

2.1.3. Dependence on surface temperature

Since the adsorption of molecules on solid surfaces varies inversely with surface temperature (T_s), one expects a slower translational energy distribution at a higher surface temperature due to a lower coverage. Fig. 10-A shows the results of photodesorption of DMCD at the temperature ranging from approximately 145 to 160 K with both surfaces using 248 nm laser radiation. The results reveal a very sharp decreases in total desorption yields by increasing the surface temperature. At T_s higher than 166 K, the signal was almost not detectable. The fitted T_{MB} with both substrates is presented in Fig. 10-B. With the quartz surface near 150 K, T_{MB} drops by more than 1000 K while the surface was heated by less than 25 K.

2.2. Product Measurements

The desorbed species resulting from photolysis at the surface were detected 13-cm from the surface in the quadrupole mass spectrometer using either EI or REMPI. The neutral species detected are H, CH₂, CH₃, CH₄, C₂H₄, C₂H₅, C₂H₆, Cd, CH₃Cd (MMCD), and (CH₃)₂Cd (DMCD). With the exception of H, which cannot be reliably measured with our present QMS setting, the TOF-distributions of these species have been measured in detail. Under higher

laser fluence conditions, particularly when the Si substrate was employed, ions were detected to desorb from the surface with much faster translational energies than those of neutral species. A similar observation was made in our earlier experiment with trimethyl gallium, in which Ga^+ ions were detected abundantly [10]. In the present experiment, an ion filter was placed between the surface and the skimmer to remove ionic species.

2.2.1. CH_3 and CH_2 radical formation

The CH_3 radical is a primary product of the gas-phase photolysis of DMCd. It can be formed by the photodissociation both at 248 nm via the $\tilde{\text{A}}$ -state excitation and at 193 nm via the $\tilde{\text{A}}$ as well as the $\tilde{\text{B}}$ -state excitation [4-8]. The possibility of CH_2 production has been ruled out by Bersohn and coworkers [8].

The photolysis of adsorbed DMCd at these wavelengths appears to have generated both CH_2 and CH_3 radicals according to the TOF-appearance times and relative counts of the m/z 14 and 15 ions under different fluence conditions. Although the relative ion yields are not quantitatively meaningful due to possible cracking contributions from larger fragments and the parent molecule, they are qualitatively useful for us to ascertain their primary origin. From Figs. 9A and 9B, it is evident that the apparent yields of CH_2^+ and CH_3^+ behave somewhat differently as the fluence of the photolysis laser is varied. This observation, together with the resolvable appearance and peak (t_{max}) times summarized in Tables 1 and 2, allows us to conclude that CH_2 radicals were produced in the surface photolysis of DMCd on quartz and silicon at both wavelengths. In Fig. 11 we have shown the deconvoluted TOF profiles obtained from the photolysis at 248 and 193 nm on the quartz surface; these profiles consist of a fast, high T_{MB} peak, a smaller component from CH_3^+ fragmentation and a very slow

component. The slowest peak is too slow to be accounted for by the fragmentation of a larger ion such as DMCd^+ . Unfortunately, the REMPI spectroscopy of CH_2 has not yet been established and thus its definitive identification can not be made at present.

The confirmation of CH_3 radicals, on the other hand, is straightforward, because CH_3 -REMPI spectroscopy is well-established [15]. Multiphoton ionization was made at 333.4 nm using the (2+1) scheme via the $3p\ ^2A_2''$ Rydberg state of the CH_3 [13,15]. The wavelength scans of the CH_3 radical formed under different conditions are shown in Fig. 12.

Figs. 13 and 14 compare the TOF profiles of the m/z 15 ion produced by both REMPI and EI methods. Although both EI and REMPI TOF profiles obtained from photolysis on the SiO_2 surface are very similar, the EI profiles are more convoluted, containing contributions from C_2H_6 and, possibly, CH_4 . These signals also show small contributions from very slow desorption processes; additionally, the peaks in the EI signals which are not present in the REMPI profiles, apparently derived from a small CH_3 -containing species. One likely candidate is CH_4 , which might be formed by the surface reaction, $\text{H(a)} + \text{CH}_3\text{(a)} \rightarrow \text{CH}_4\text{(g)}$.

In Fig. 14, we have compared the CH_3 EI/TOF-profiles measured with photolysis at 248 and 193 nm using the quartz substrate. The 248-distribution is not only colder, but also contains a much larger contribution from the slow desorption process with $T_{\text{MB}} \sim 50$ K.

2.2.2. C_2 Formation

As shown in Figs. 1 and 2, C_2H_4 , C_2H_5 and C_2H_6 have distinctly different TOF-profiles from those of DMCd . Accordingly, they are primarily the products

of surface photochemical reactions, with very minor contributions from the fragmentation of DMCd^+ .

Among the three C_2 products, C_2H_4 has the highest ion yield, but its TOF profile tracks closely with that of C_2H_6 and the relative ratio of $\text{C}_2\text{H}_4^+/\text{C}_2\text{H}_6^+$ remains constant and is close to the C_2H_6^+ fragmentation pattern. Thus, C_2H_4^+ derives mainly from C_2H_6^+ .

C_2H_6 is most likely the product of the surface reaction, $2 \text{CH}_3 (\text{a}) \rightarrow \text{C}_2\text{H}_6(\text{g})$. Its desorption profiles are distinctly different from those of DMCd , the only heavier photodesorption product which can possibly generate a C_2H_6^+ ion by ion-fragmentation. The parent DMCd^+ ion, however, produces very little $m/z=30$ ion fragment as indicated in Figs. 3 and 4. Similar to the photodesorption of DMCd , the observed translational temperature of C_2H_6 is much hotter from 193 nm photolysis than 248 nm irradiation. With 20 mJ/cm^2 .pulse fluence, for example, $T_{\text{MB}} = 542 \text{ K}$ at 248 nm, in comparison with 777 K at 193 nm. Both profiles presented in Fig. 15 reveal the presence of slow desorption processes which will be addressed later.

The C_2H_5 profiles differ somewhat from those of C_2H_6 . This is most apparent from the photolysis on quartz with both lasers as shown in Fig. 16. The photolysis with the 193 nm laser generates a higher C_2H_5^+ ion yield, with the major contribution from C_2H_6 , which derives from the abundant CH_3 radicals produced by the photolysis at this wavelength. At 248 nm, C_2H_5^+ ion yield is much lower, because the surface concentrations of CH_3 and CH_2 , possible precursors of C_2H_5 , are comparatively lower.

2.2.3. Cd and CH₃Cd Formation

As shown in Figs. 3 and 4, both Cd and CH₃Cd are major ion fragments of DMCd. We therefore attempted to resolve the observed TOF-distributions with careful deconvolution, and, in case of Cd, an additional REMPI detection was employed, as illustrated in Fig. 17.

In Fig. 18, the TOF-distributions of Cd⁺ ($m/z = 114$) were obtained by the photolysis of 0.009 ML DMCd on quartz with 248 nm radiation; both EI and REMPI ionizations were utilized in the mass analysis. The distribution obtained by REMPI can be quantitatively characterized by a Maxwell-Boltzmann distribution with $T_{MB} = 458$ K. The distribution obtained by EI, on the other hand, contains two components; one from the desorbed Cd atom (46%, $T_{MB} = 458$ K) and the other from the desorbed DMCd (54%, $T_{MB} = 479$ K). The deconvoluted results for the neutral Cd are summarized in Tables 1 and 2 for the photolysis on quartz with both 193 and 248 nm, respectively.

The REMPI spectroscopy of CH₃Cd has not yet been established. We detected it ($m/z = 129$) entirely by EI. Figure 19 presents the TOF-distributions of the m/z 129 ions generated from the products of adsorbed DMCd on quartz, photolyzed at 193 and 248 nm. Since CH₃Cd⁺ can derive from CH₃Cd and/or DMCd, the deconvolution process is relatively straightforward. The result of the analysis indicates that in the 248 nm photolysis, the DMCd fragmentation is small, the CH₃Cd⁺ ion signal derives almost entirely from DMCd⁺ ion fragmentation. The 193 nm photolysis, on the other hand, resulted in more fragmentation at the surface, about 13% of the CH₃Cd⁺ signal apparently derives from the desorbed CH₃Cd radical. We hope to confirm this observation by REMPI when we return to study the deposition of CdS and CdTe films in the near future.

3. Discussion

The photodissociation of dimethyl cadmium, adsorbed on a quartz and a silicon(111) substrate, with 193 and 248 nm radiations results in both fragmentation and desorption. Detected species include H, CH₂, CH₃, CH₄, C₂H₄, C₂H₅, C₂H₆, Cd, CH₃Cd and (CH₃)₂Cd.

The translational temperatures (T_{MB} 's) of the desorbed species typically increase with surface coverage, photon energy (248 vs. 193 nm) and laser fluence, as presented in detail in the preceding section. The intensity as well as T_{MB} 's of desorbed products are much higher with the silicon substrate than with the quartz substrate, presumably attributable to higher surface coverage and absorptivity of the UV radiations by the former. Both possibilities can contribute to larger desorption yields and higher T_{MB} values as shown in Figs. 2 and (6B).

Since both quartz and Si(111) data are qualitatively similar, most detailed mechanistic analyses were carried out with the quartz data. The results of these analyses are discussed below.

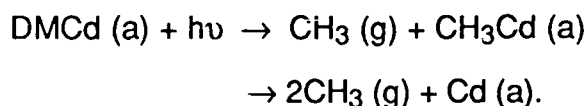
3.1. Photodissociation Mechanism:

The mechanism of the photodissociation of adsorbed DMCd, based on the data presented in the preceding section, is summarized in Fig. 20. This surface photolysis mechanism is very different from that of the gas phase one which consists of CH₃, CH₃Cd and/or Cd as the primary fragmentation products when DMCd is excited at the \tilde{A} or the \tilde{B} state [4-8].

The photolysis of DMCd on solid surfaces leads not only to additional fragmentations of CH₃ and CH₃Cd, but also to the formation of recombination products aided by the surface. This unambiguous conclusion was made possible by the additional REMPI detection of CH₃ and Cd as illustrated in Figs.

12/13, and 17/18, respectively. The quantification of CH₃ and Cd TOF-distributions allows us to deconvolute the TOF-distributions of CH₂, CH₃ and Cd obtained by EI/MS quite reliably. The deconvoluted relative contributions to various species are tabulated in Tables 3 and 4 for photolysis on quartz at 193 and 248 nm, respectively, under the same fluence and dosage conditions.

Our definitive determination of the TOF-distributions of CH₃ by REMPI/MS also allows us to rule out the possibility of the direct production of the radical without surface mediation, such as

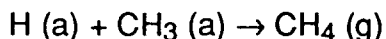
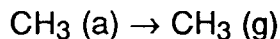
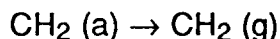
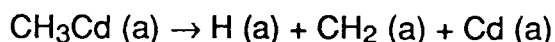
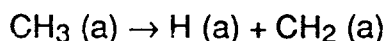
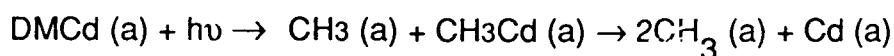


The average translational energies ($\langle E_t \rangle = m\langle v \rangle^2/2$) of the CH₃ radical measured in the 193-nm photolysis on quartz, with a typical dosage of 0.03 L, ranges from 3.8 to 7.4 kJ/mole, when laser fluence is varied from 11 to 20 mJ/cm² (see the data presented in Table 1). This range of $\langle E_t \rangle$ is significantly lower than that reported by Bersohn and coworkers [8], 24.3 kJ/mole, in their gas-phase photolysis of DMCd at 193 nm using a comparable fluence of 2 MW/cm² (which is approximately 20 mJ/cm² for a typical ArF-excimer laser with a pulse-width of about 10 nsec). Since the adsorption energy of DMCd on quartz is expected to be significantly smaller than the excitation energy (i.e., the amount of available energy for DMCd fragmentation on the surface and in the gas phase should be about the same), the low values of $\langle E_t \rangle$ measured in the present study, suggest clearly that the production of CH₃, similar to all other desorbed species, is surface-mediated.

3.1.1. C₁-Products

The major C₁-products detected are CH₂, CH₃ and CH₄ as shown in Figs. 11, 13 and 14. CH₄ appears as an early shoulder in the EI spectra presented in these figures.

The three C₁- products are most likely formed by the following processes during or after the photolysis on the surface:



Both CH₂(a) and CH₃(a) desorb at about the same time, but the deconvoluted CH₂ signal, which is larger from 193 nm than from 248 nm photolysis, has a slightly higher translational energy (see Tables 1 and 2 and Fig. 11) than that of CH₃. Under a typical exposure of 0.03 L on quartz, for example, T_{MB} (CH₂) = 520 K vs. T_{MB} (CH₃) = 465 K at 248 nm, and T_{MB} (CH₂) = 775 K vs. T_{MB} (CH₃) = 697 K at 193 nm.

Interestingly, as can be seen in Figs. 11, 13 and 14, all CH₂ and CH₃ TOF-distributions, including the ones obtained by REMPI for CH₃, contain very slow, cold tails. These slow desorbing components probably derive from the species (CH₂ or CH₃), which migrate into the desorption site aligned with the detection axis (i.e. the line-of-sight) via diffusion. These components are too cold to be attributed to MMCd or DMCd.

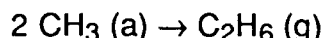
The m/z -15 REMPI signal can be accounted for entirely by the described CH_3 radicals; the observed wavelength scans summarized in Fig. 12 agree quantitatively with those measured in the pyrolysis of $(\text{CH}_3)_2\text{SO}$ or $[(\text{CH}_3)_3\text{CO}]_2$ [13]. The signals obtained by EI given in Figs. 13 and 14, however, contain an early observable shoulder, which has been ascribed to CH_4 , and a slower component (10-15%) derived from the fragmentation of C_2H_6^+ . As indicated above, the very cold tails appear in these figures, cannot be accounted for by either MMCd^+ or DMCd^+ fragmentation; the TOF-distributions of either Cd-containing species are quantitatively characterizable as will be discussed below.

According to the total ion counts presented in Figs. 9A and B, the $m/z = 15$ signals are the largest produced by 193 nm photolysis. The signal intensities appear to decline noticeably under high fluence conditions. This is particularly evident with the Si substrate. The decline in the yields of CH_3 and other neutral desorption products under high fluence conditions correlates strongly with the observed ion yields, detectable with the EI filament turned off. Ions were more abundantly produced on the Si than the quartz substrate, as one would expect. To eliminate these ions, an ion filter was placed in front of the skimmer in the course of our experiments as alluded to before.

3.1.2. C_2 - Products

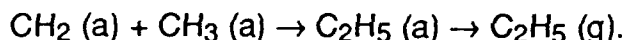
In our EI/MS analyses of desorbed products, three C_2 - containing ions were detected, $m/z = 28, 29$ and 30 , which can be attributed to C_2H_4^+ , C_2H_5^+ and C_2H_6^+ . Their TOF - distributions are presented in Figs. 1, 2, 15 and 16. As discussed in section 2.2.2, C_2H_4^+ TOF-distributions follow closely with those of C_2H_6^+ ; it probably results primarily from C_2H_6^+ fragmentation.

The m/z -30 signal derives exclusively from C_2H_6 , which is most certainly the product of the CH_3 recombination reaction on the surface:



Similar to the C_1 - products, the TOF - profiles C_2H_6 also contain a fast component (~75 - 85 %) desorbing directly from the region of the substrate aligned with the QMS analysis axis and a much slower component desorbing after migration into the line-of-sight. This component is also too slow to be accounted for by DMCd, the only heavy species which may contribute to the m/z - 30 signal. The translational temperature of C_2H_6 is comparable to those of the C_1 - products as summarized in Tables 1 and 2.

C_2H_5 derives probably from the recombination process:



After subtracting the contribution from C_2H_6 , the deconvoluted profiles differ distinctly from those of C_2H_6 , which can be relatively cleanly characterize as indicated above. The translational temperature of C_2H_5 is much colder than that of C_2H_6 , reflecting the possibility that the rate of C_2H_5 formation on the surface is much slower, due to the lower concentration of CH_2 (a).

3.1.3. Production of Cd, CH_3Cd and $(CH_3)_2Cd$

As a group, Cd, MMCd and DMCd appear with similar TOF-distributions (see Figs. 1, 2, 18 and 19) and are also associated high translational temperatures. Their T_{MB} 's are typically twice as high as those of C_1 - and C_2 - products, suggesting that substantial electronic excitation/relaxation might have

contributed to their desorption processes. This is perhaps not unexpected because ions have been generated from the photolysis. In our previous study of the photodissociation of adsorbed trimethylgallium on quartz and LiF (001) substrates, the desorbed Ga atom was also measured to have a much higher translational temperature than the CH_3 radical [10]. Both species were detected by REMPI/MS. In this case, Ga^+ ions were also detected to desorb from the deposited Ga film.

As shown in Figs 17 and 18, the Cd atom could be readily and selectively detected by REMPI/MS. The REMPI TOF-profiles can be quantitatively characterized by Maxwell-Boltzmann temperatures without interference from MMCd or DMCd. The EI TOF - profiles, on the other hand, was found to contain the fraction from DMCd. The deconvoluted result shown in Fig. 18, for example, indicates that as much as 54 % of the Cd signal derived from DMCd^+ when DMCd (a) was photolyzed at 248 nm. A much lower fraction of contribution from DMCd was observed with 193 nm photolysis as one would expect. Since most measurements were carried out with EI analysis, deconvolution is required to quantify Cd-distributions; the deconvoluted temperatures under various conditions using the quartz substrate are summarized in Tables 1 and 2. It should be mentioned that the contribution of MMCd^+ to the Cd^+ signal was found to be negligible because of the low desorption yield of MMCd as discussed below.

The measured monomethyl cadmium, MMCd, signals were concluded to derive almost exclusively from DMCd, even when photolysis was carried out at 193 nm, at which the absorption of the laser radiation by DMCd is expected to be stronger. The result shown in Fig. 19, obtained from the photolysis of 0.03 L DMCd with a fluence of $20 \text{ mJ/cm}^2\text{.pulse}$, indicates an estimated 13% MMCd contribution to the observed MMCd^+ signal, which has a factor two colder T_{MB}

value than DMCd. The slow desorption velocity of MMCd may suggest a stronger binding of the CH_3Cd radical with the deposited Cd film.

DMCd, the parent molecule, possesses the highest translational temperature measured. This temperature was found to be affected strongly by photon energy, surface coverage, laser fluence as well as the nature of the surfaces employed. Since the studies on these effects were performed most extensively with the DMCd desorption process, the results of these studies are discussed separately below.

3.2. Photon Energy Dependence

The measured translational energies of all desorbed species, including DMCd, were consistently higher with 193-nm than 248-nm photolysis. As shown in Tables 1 and 2, the results of the photolysis on quartz at the same fluence of $20 \text{ mJ/cm}^2\text{.pulse}$, T_{MB} 's for all products were higher by 30-40% with the former wavelength, at which the photon energy is higher by 137 kJ/mole and the absorption by DMCd is expected to be stronger as well. The excess photon energy, apparently, could be utilized by photofragments for more efficient desorption.

Another factor, which may also affect the desorption efficiency, is surface heating by the photolysis laser. Although the UV-grade fused silica used in the present experiment is highly transparent to 193 and 248 nm, particularly the latter, the deposited Cd film may strongly alter the transmission of these radiations under steady photolysis conditions. To examine this effect further, we have studied the dependence of desorption yields as functions of laser fluence as discussed in the following section.

The high translation energy of desorbed DMCD observed at both photolysis wavelengths may due in large part to the strong coupling of electronic excitation/surface relaxation processes which are unavailable to small alkyl fragments.

3.3. Laser Fluence Dependence

The intensity of photolysis laser has been shown to increase the translational energy of desorbed species [16-21]. For desorption from LiF surfaces, such an enhancement effect has been attributed to the increase in the intensity of photoacoustic wave induced by F-center excitation at higher fluences [16-18]. For optically opaque substrates, surface heating becomes important.

In the present case, the results of photolysis on the quartz substrate at 193 and 248 nm under varying fluence conditions are summarized in Tables 1, 2, and Figs. 7 and 8. For the desorption of DMCD, the leveling off of the T_{MB} value at high fluences indicates the absence of a two-photon excitation process. The initial rapid increase in T_{MB} with fluence may be due to both enhanced surface heating and desorption yield, which may contribute to the narrowing of the cone of desorption to be described below on surface coverage dependence.

3.4. Surface Coverage Dependence

The results summarized in Figs. 5 and 6 show unambiguously that not only the desorption yield but also translational temperature of DMCD was strongly affected by exposure or surface coverage. Similar observation have been reported in many laser-desorption studies [16-21].

Polanyi and coworkers have studied in detail the angular dependence of desorption yields on surface coverage [16, 18]. For the OCS desorption from LiF (001), for example, they observed a sharp variation in the angular distribution from $\cos \theta$ with $\sim 10^{-3}$ L exposure to $\cos^{11} \theta$ with 21 L exposure [18]. The enhancement of the desorption yield toward surface normal at higher coverages is believed to result from the reduction in "the thermal liberation of the adsorbate-surface bond and the permitted cone-of-escape angles for photodesorption product" [18]. The sharp increase in T_{MB} and desorption yield with surface coverage, as shown in Fig 6 would suggest that a considerable energy and momentum transfer occurs at or near the surface during the desorption process.

3.5. Extent of Film Deposition

After the completion of this series of surface photochemical experiments, both SiO_2 and Si (111) were analyzed with x-ray photoelectron spectroscopy. The result of this analysis indicated that very little Cd metal was deposited on the substrates. This finding suggests that under the fluence of $\sim 20 \text{ mJ/cm}^2$ pulse (15 nsec), Cd could be very efficiently removed from these solid substrates. We hope to study the effect of group VI elements on the formation of II/VI semiconductive films under the influence of similar laser intensities.

4. Conclusions

The photolysis of $(\text{CH}_3)_2\text{Cd}$, adsorbed on quartz and Si(111) substrates at submonolayer levels, with ArF (193 nm) and KrF (248 nm) lasers was found to desorb as well as to fragment the $(\text{CH}_3)_2\text{Cd}$ molecule. Products detected by

time-of-flight mass spectrometry, using either electron impact ionization (for all species) or resonance-enhanced multiphoton ionization (for Cd and CH₃), are H, CH₂, CH₃, CH₄, C₂H₄, C₂H₅, C₂H₆, CH₃Cd and (CH₃)₂Cd.

Both the measured yields and fitted Maxwell-Boltzmann temperatures of these products (except H) were found to increase with surface coverage, laser fluence and photon energy. The desorbed hydrocarbon products, C₁- and C₂-species, typically have about the same translational energies, which are significantly lower than those of the Cd - containing ones; ie, Cd, CH₃Cd and (CH₃)₂Cd. This observation was attributed to the coupling of the electronic excitation/surface relaxation process to desorption, giving rise to the more efficient and energetic desorption process for the metal-atom containing species. The electronic excitation of the adsorbed organometallic species and the deposited metal film can occur quite readily. In fact, copious amounts of ions were detected at higher-fluences, under which the yields of neutral products (through ion filtration) were found to drop noticeably. The analysis of the photolyzed surfaces under these high fluence conditions revealed very little Cd deposition on both SiO₂ and Si(111) substrates. A detailed mechanism for the photodesorption/photodecomposition of (CH₃)₂Cd adsorbed on these solid surfaces is proposed.

Acknowledgment

The authors grateful acknowledge the support received from the Office of Naval Research under contract No. N00014-89-J-1235. We also thank Dr. Y. He for carrying out a preliminary experiment of this study.

References

1. D. Bauerle, Chemical Processing with Lasers, Springer-Verlag, 1986.
2. R. M. Osgood, Jr., Ann. Rev. Phys. Chem. 34, 77 (1983).
3. C. D. Strinspring and A. Freedman, Chem. Phys. Lett. 143, 584 (1988).
4. C. J. Chen and R. M. Osgood, Jr., J. Chem. Phys. 81, 327 (1984).
5. A. Amirav, A. Penner and R. Bersohn, J. Chem. Phys. 90 5232 (1989).
6. T. Ibuki, A. Hiraya and K. Shobatake, J. Chem. Phys. 92, 2797 (1990).
7. M. Suto, C. Ye and L. C. Lee, J. Chem. Phys. 89, 160 (1988).
8. C. F. Yu, F. Youngs, K. Tsukiya, R. Bersohn, and J. Presses, J. Chem. Phys. 85, 1382 (1986).
9. T. F. Deutsch, D. J. Erlich and R. M. Osgood, Jr., Appl. Phys. Lett. 35, 175 (1979).
10. E. Villa, J. A. Dagata and M. C. Lin, AIP Conf. Proc. No. 191, Adv. Laser Sci. IV., p. 379, Am. Inst. Phys., 1989.
11. E. Villa, J. A. Dagata, and M. C. Lin, J. Chem. Phys. 92, 1407 (1990).
12. J. A. Dagata, E. Villa and M. C. Lin, Appl. Phys. B.51, 443 (1990)..
13. J. W. Hudgens, T. G. DiGiuseppe and M. C. Lin, J. Chem. Phys. 79 571 (1983).
14. C. E. Moore, Atomic Energy Levels, vol. IV. p. 55, NSRDS-NBS35, National Bureau of Standards, U. S. Department of Commerce, 1971.
15. M. C. Lin and W. A. Sanders, in Adv. in Multiphoton Processes and Spectroscopy, S. H. Lin, Ed., vol. 2 p. 333, World Scientific Pub. Co., Singapore, 1986.

16. I. Harrison, J. C. Polanyi and P. A. Young, J. Chem. Phys. 89 1475, 1498 (1988).
17. St. J. Dixon-Warren, K. Leggett, M. S. Matyiaszczyk, J. C. Polanyi and P. A. Young, J. Chem. Phys., 93, 3659 (1990).
18. J. C. Polanyi and P. A. Young, J. Chem. Phys. 93, 3673 (1990).
19. K. Domen and T. J. Chuang, J. Chem. Phys. 90, 3318, 3332 (1989).
20. F. L. Tabares, E. P. Marsh, G. A. Back and J. P. Cowin, J. Chem. Phys. 86, 738 (1987).
21. Y. Bu, S.-P. Lee and M. C. Lin, "Photodesorption of adsorbed benzene from LiF(001) by Selective Excitation at 308, 248 and 193 nm". to be published.

Table 1. Photofragments and Desorption Products from the 193-nm
Photolysis of Adsorbed Dimethyl Cadmium on Quartz at 143 K.^a

Laser Energy	M/Z (amu)	Ion Counts	τ_{\max} (μ sec)	T _{MB} (K)
11.0	14	30621	148	N/A ^b
	15	105631	151	355
	28	68663	199	(c)
	29	13458	199	175
	30	20934	205	376
	114	7578	326	N/A
	129	17400	335	N/A
	144	54329	336	666
12.8	14	51304	122	508
	15	168916	131	470
	28	169657	167	(c)
	29	39100	173	293
	30	55419	162	598
	114	27536	251	584
	129	82103	252	590
	144	54329	225	1485
16.8	14	86237	104	698
	15	339333	111	665
	28	270080	145	(c)
	29	79513	142	144
	30	73576	149	711
	114	87010	208	1170
	129	188519	216	965
	144	114779	201	1909
20.4	14	117899	98	777
	15	385859	108	697
	28	312612	140	(c)
	29	84346	143	201
	30	89078	142	777
	114	134430	197	1605
	129	227615	207	1328
	144	117981	199	1920

a. The DMCd exposure was typically 0.03 L.

b. Not available.

c. C₂H₄⁺ derives entirely from C₂H₆⁺.

Table 2. Photofragments and Desorbed Products from the 248-nm Photolysis of Adsorbed Dimethyl Cadmium on Quartz at 143 K.^a

Laser Energy	M/Z	Ion Counts	τ_{\max} (μsec)	T_{MB} (K)
20.6	14	28247	121	522
	15	58928	133	465
	28	31527	172	N/A ^b
	29	14321	188	248
	30	10405	171	531
	114	46931		1001
	129	117766	260	(d)
	144	71145	261	1115
22.7	14	41857	114	594
	15	118247	124	527
	28	60074	167	(c)
	29	28617	183	276
	30	17356	168	566
	114	94042	231	1190
	129	217966	241	(d)
	144	144352	236	1360
24.0	14	44678	107	684
	15	130932	118	584
	28	N/A		N/A
	29	30982	183	293
	30	17429	161	610
	114	109618	218	1360
	129	232003	229	(d)
	144	160370	225	1508
26.7	14	61318	99	808
	15	194929	110	677
	28	74086	151	(c)
	29	46271	177	298
	30	22289	153	684
	114	158853	209	1560
	129	337517	216	146
	144	168090	219	1591
28.9	14	49439	107	664
	15	147147	118	580
	28	72921	161	(c)
	29	37481	166	272
	30	23322	161	612
	114	128960	219	1360
	129	286776	228	241
	144	172731	226	1483

(a), (b), (c), see footnote given in Table 1.

(d) DMCd⁺ fragment.

Table 3. Boltzmann temperatures, contributions from other heavier species and total ion counts of all observed species from the 193nm photolysis of DMCd adsorbed on a cold quartz surface (20 mJ/cm²-pulse and 0.03 L).

Observed Ions	m/z:	14	15	28	29	30	114	129	144
T _{MB} /K		777	697		201	777	1605	1328	1920
(Counts)		105368	390767	312612	84346	89078	134248	228571	117981
CH ₂	0.88								
CH ₃	0.12		0.95						
C ₂ H ₄									
C ₂ H ₅					0.21				
C ₂ H ₆			0.05	1	0.79	1			
Cd							0.73		
MMCd								0.68	
DMCd							0.27	0.32	1

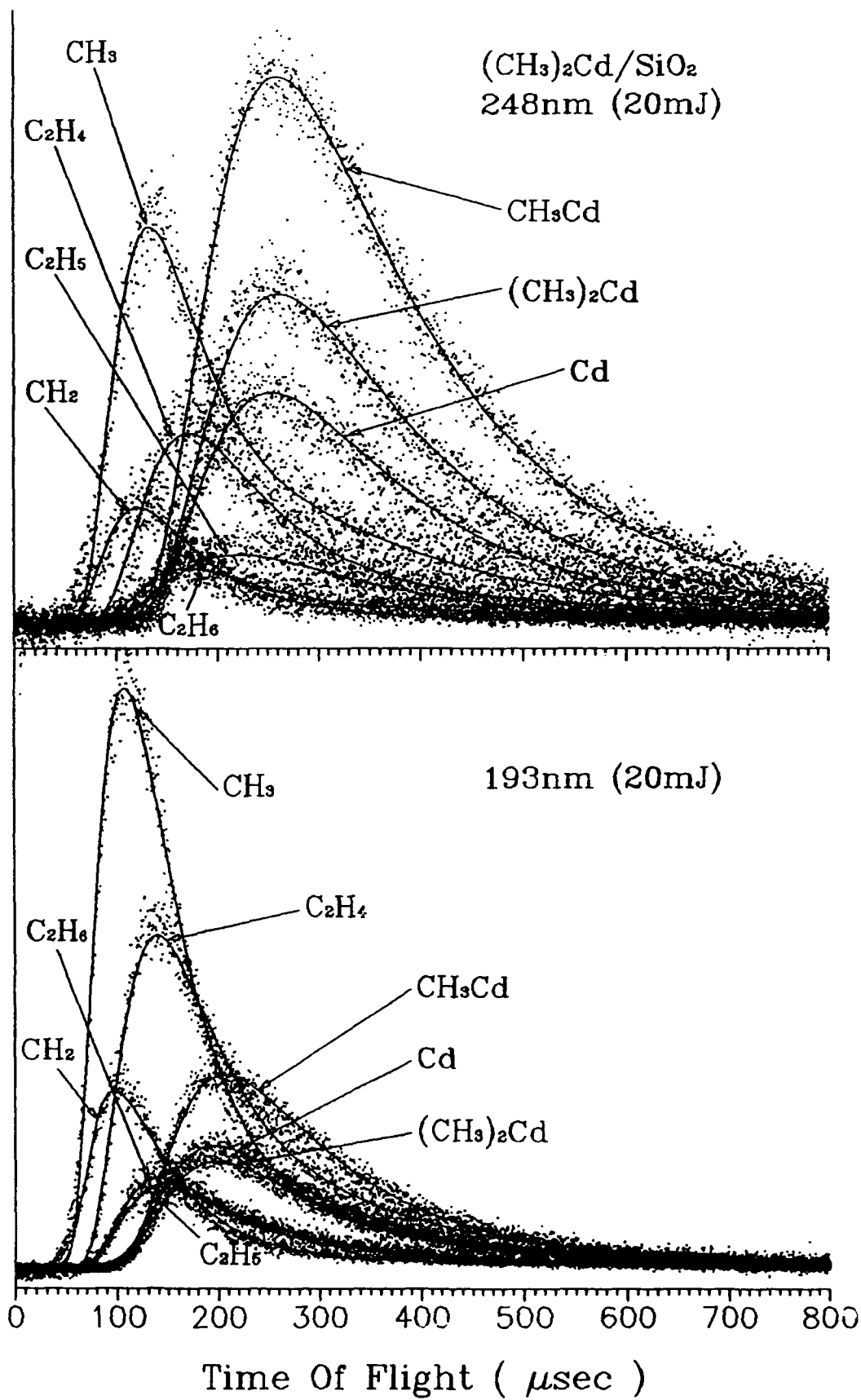
Table 4. Boltzmann temperatures, contributions from other heavier species and total ion counts of all observed species from the 248nm photolysis of DMCd adsorbed on a cold quartz surface (20 mJ/cm².pulse and 0.03 L).

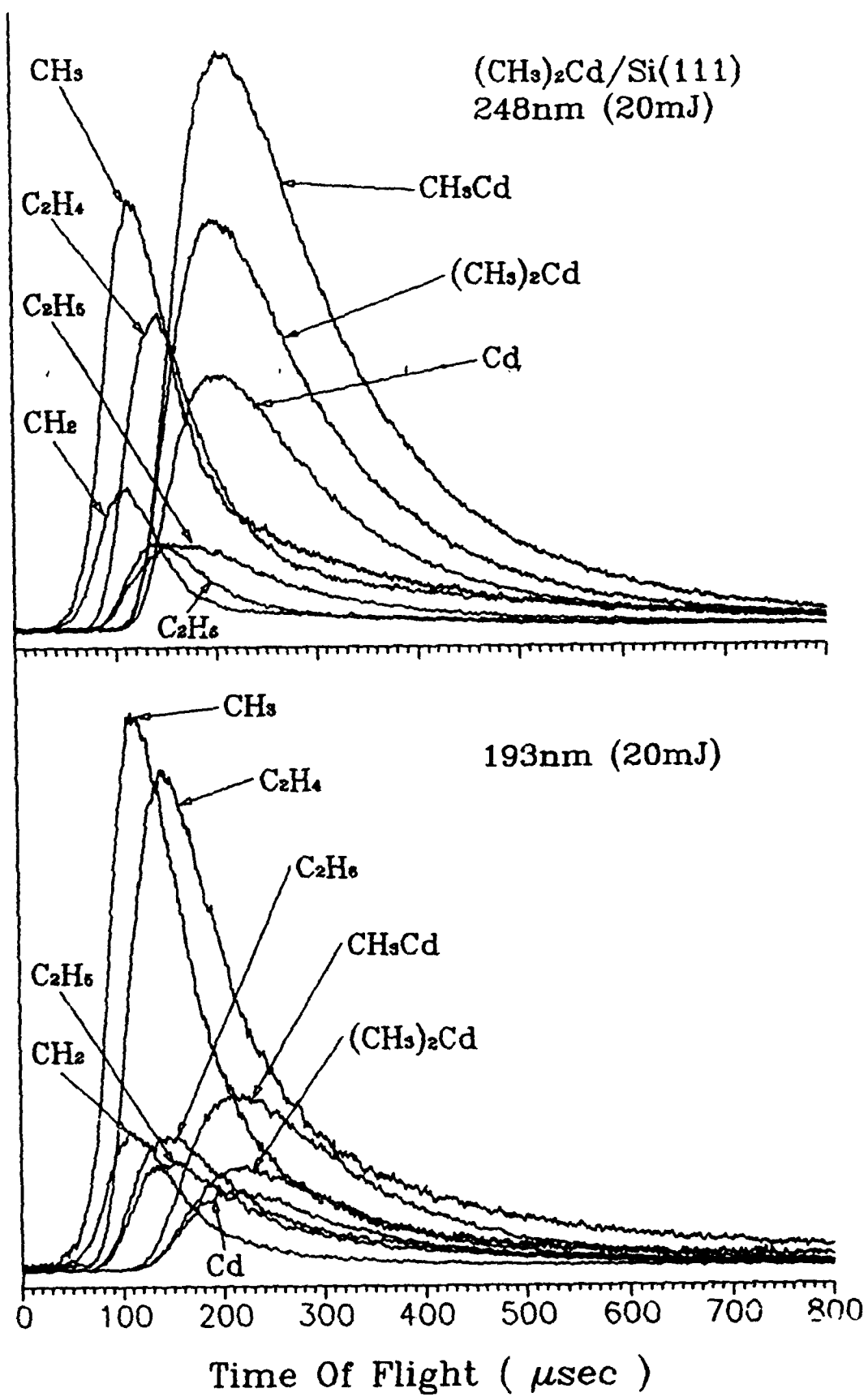
Observed Ions	m/z:	14	15	28	29	30	114	129	144
T _{MB} /K		522	465		248	531	1001		1115
(Counts)			59201	31527	14321	10405	46931		117981
CH ₂	0.62								
CH ₃	0.37		0.33						
C ₂ H ₄									
C ₂ H ₅					0.69				
C ₂ H ₆			0.07	1	0.31	1			
Cd							0.46		
MMCd								0.04	
DMCd							0.54	0.96	1

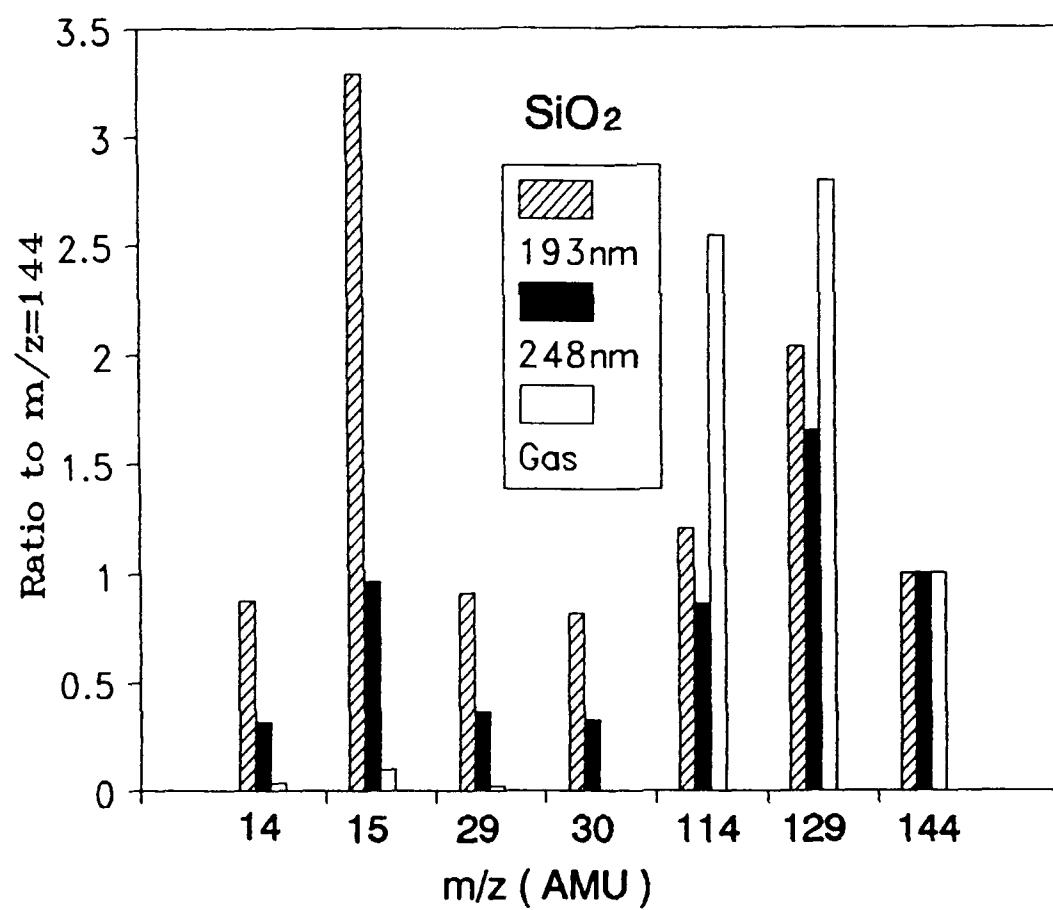
Figure Captions

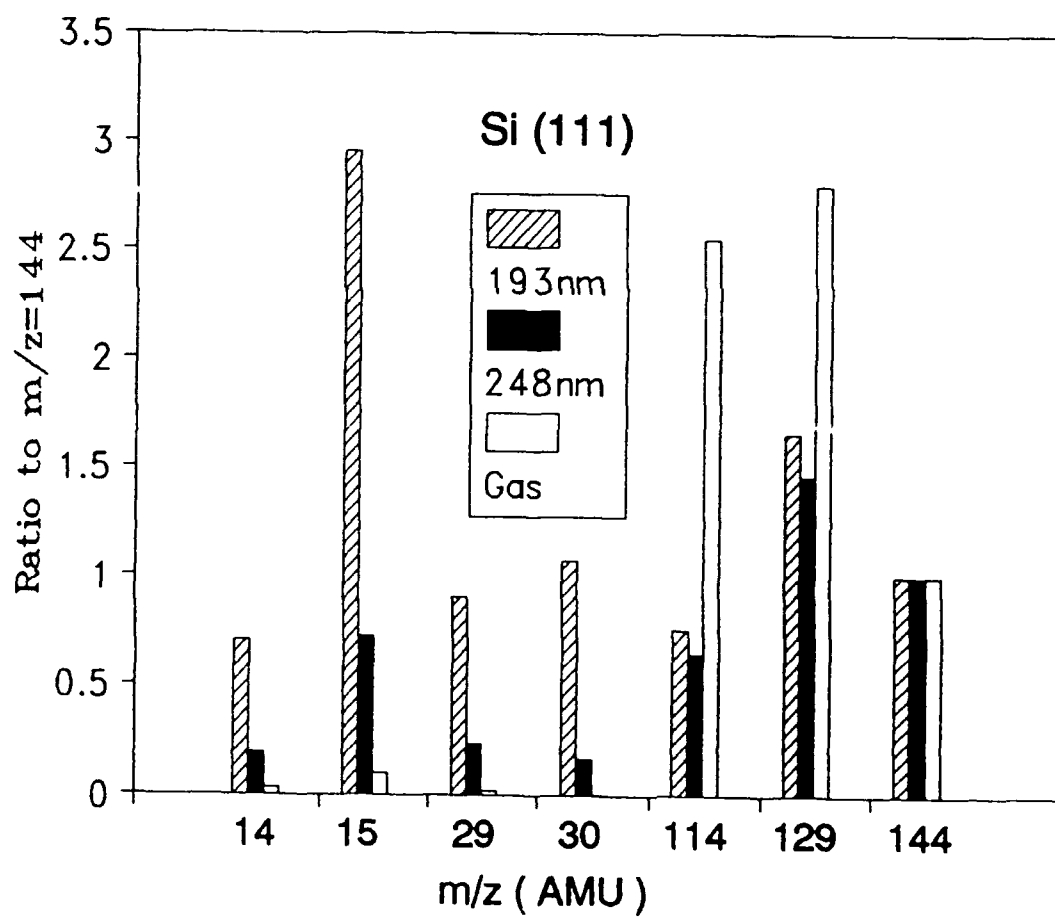
1. Overall view of the flight times of the products of DMCd on SiO₂ by 193- and 248-nm irradiation. The fluence for both wavelengths was 20 mJ/cm².pulse and the surface exposure was maintained at 0.03 L. The superimposed solid lines are fitted Maxwell-Boltzmann distributions.
2. Overall view of the flight time of the products of photodesorption/photo-fragmentation of DMCd on Si(111) by 193- and 248-nm irradiation. The fluence for both wavelengths was 20mJ/cm².pulse and the surface exposure was maintained at 0.024 L.
3. Comparison of total ion-count distributions of observed species from the photolysis of adsorbed DMCd on SiO₂ at 193 and 248nm, using the same fluence (20mJ/cm²pulse), with the ion-fragmentation pattern of DMCd detected in the gas phase. The ion counts were normalized with respect to the parent (DMCd) counts.
4. Comparison of total ion-count distributions of observed species from the photolysis of DMCd on Si(111) at 193 and 248nm, using the same fluence (20mJ/cm²pulse), with the ion-fragmentation pattern of DMCd detected in the gas phase. The ion counts were normalized with respect to the parent (DMCd) counts.
5. Representative TOF profiles of the photodesorbed DMCd from the SiO₂ surface at different exposures by 248 nm irradiation with 29mJ/cm².pulse fluence.
- 6A. Dependences of the total desorption count and translational temperatures of the photodesorbed DMCd from the SiO₂ surface on the exposure photolyzed at 248 nm with 29 mJ/cm².pulse fluence.
- 6B. Dependences of the total desorption count and translational temperatures of the photodesorbed DMCd from the Si(111) surface on the exposure photolyzed at 248 nm with 29 mJ/cm².pulse fluence.
7. Comparison of changes in TOF profiles of photodesorbed DMCd with laser fluence between 193 and 248 nm radiations. The surface exposure was 0.03 L.
8. Comparison of translational energy distributions of photodesorbed DMCd molecules between 193 and 248 nm radiations.
- 9A. Overall comparison of total ion counts of photodesorbed species from the photolysis of DMCd on SiO₂ at different laser fluences.
- 9B. Overall comparison of total ion counts of photodesorbed species from the photolysis of DMCd on Si(111) at different laser fluences.

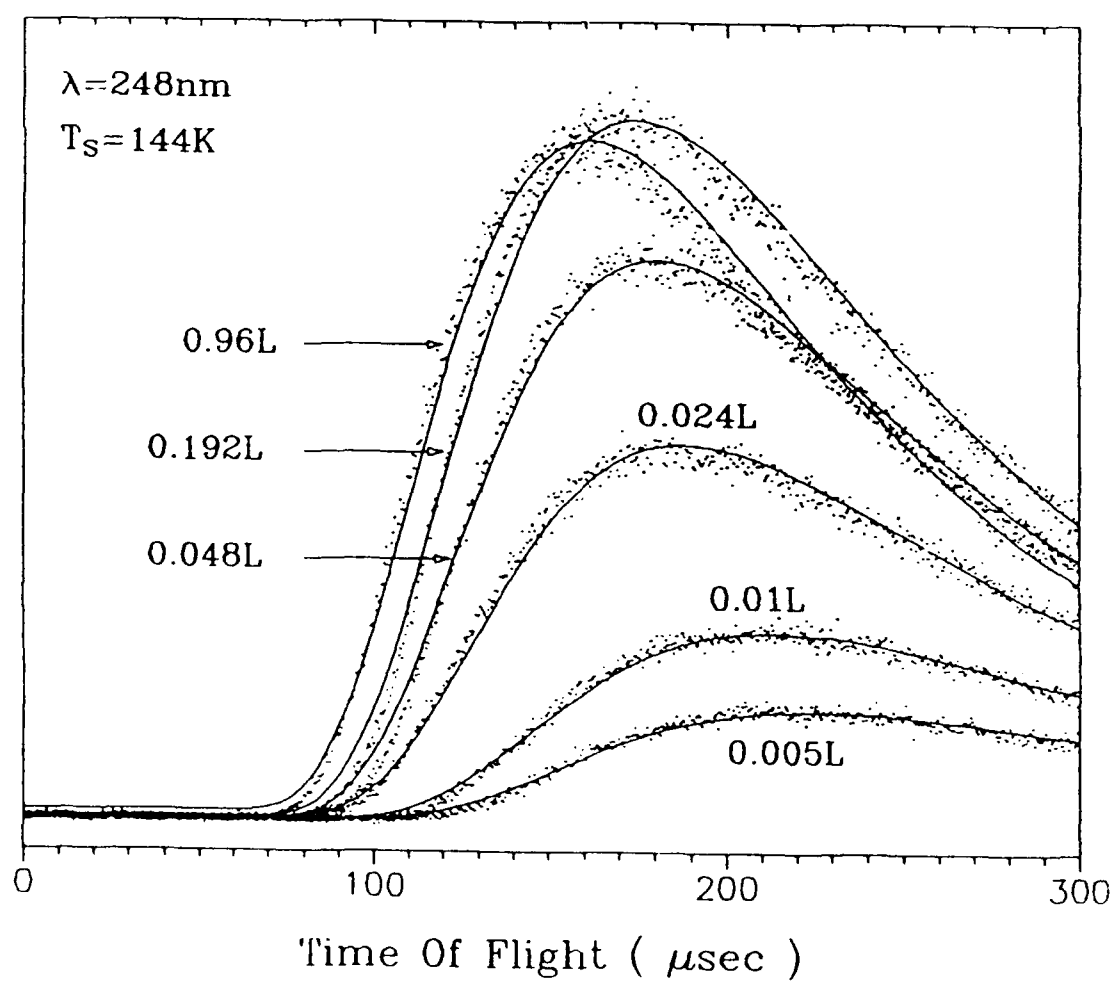
- 10A. The dependence of TOF-profiles and desorption yields of DMCd on both quartz and Si(111) surfaces photolysed at 248 nm.
- 10B. The dependence of T_{MB} of desorbed DMCd from both SiO₂ and Si(111) on surface temperature. The exposures were 0.03 L for SiO₂ and 0.024 L for Si(111); the laser was operating at 248 nm with 26 mJ/cm².pulse.
11. Comparison of EI/TOF profiles of CH₂ produced by 193 and 248 nm photolyses. The deconvoluted profiles are shown by solid curves.
12. (2+1) REMPI spectra of CH₃ radicals obtained under different conditions (Dosage = 0.03 L, fluence = 20 mJ/cm².pulse).
13. TOF profiles of photodesorbed CH₃ radicals from the SiO₂ surface detected by two different methods under the same conditions (photofragmented by 248 nm at 26 mJ/cm².pulse and the surface exposed at 0.005 L).
14. Comparison of EI/TOF profiles of CH₃ including contributions from C₂H₆ between 193 and 248 nm radiations.
15. TOF profiles of C₂H₆ from SiO₂ surface photolysis. Solid lines show the fitting with two Maxwell-Boltzmann distributions.
16. TOF profiles of C₂H₅ from SiO₂ surface photolysis including contributions from C₂H₆.
17. REMPI spectra of the photofragmented Cd from SiO₂ at two different photolysis wavelengths (see the text for line identification).
18. TOF profiles of photofragmented Cd from SiO₂ detected by two different methods under the same conditions. Upper: selectively detected by (2 + 1) REMPI at 337.7 nm. Lower: detected by electron impact ionization including contribution from DMCd. Photofragmented at 248 nm with 26 mJ/cm².pulse fluence and surface exposure, 0.005 L.
19. TOF profiles of MMCd from photolysis at 193 and 248 nm on the SiO₂ substrate, including contributions from DMCd.
20. Mechanism of the photodesorption and photofragmentation of DMCd adsorbed on solid substrates by UV laser irradiation.





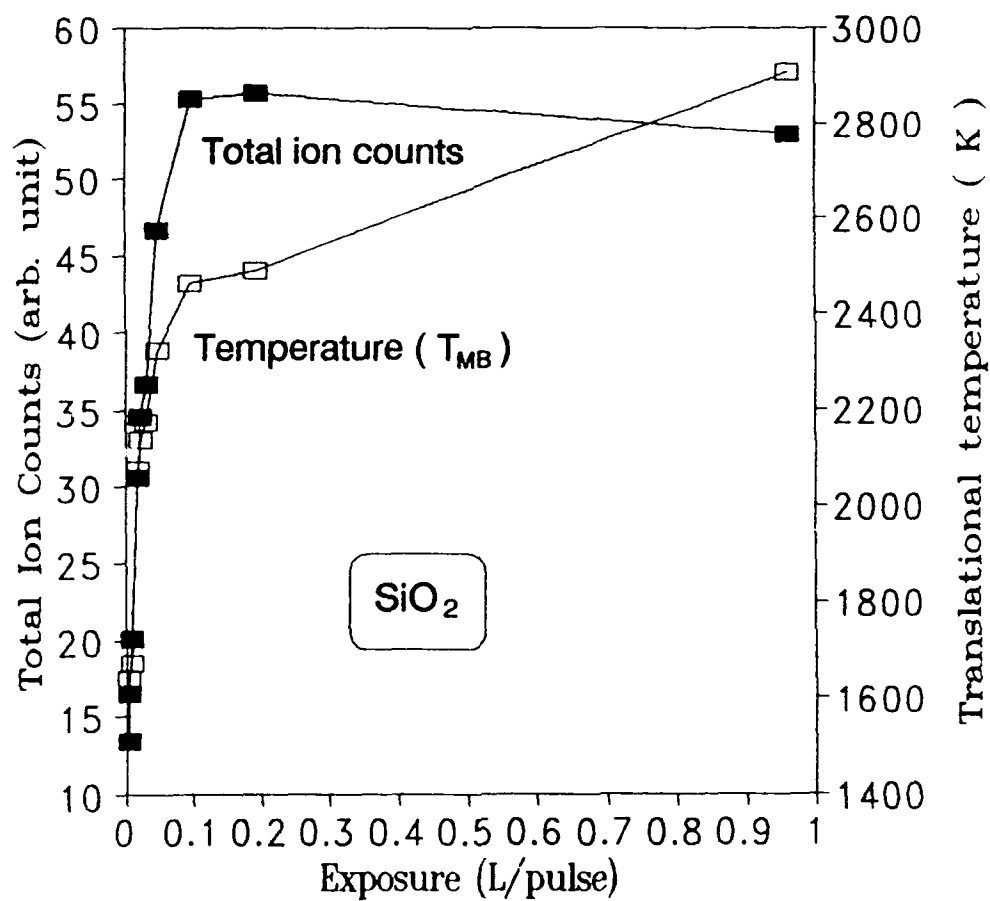






6A

Exposure dependence of $m/z=144$ from Quartz at 144K



Exposure dependence of $m/z=144$
from Si(111) at 141K

